
WELL-POSEDNESS STUDY OF A NON-LINEAR HYPERBOLIC-PARABOLIC COUPLED SYSTEM APPLIED TO IMAGE SPECKLE REDUCTION

A PREPRINT

Sudeb Majee
School of Basic Sciences
Indian Institute of Technology Mandi
PIN 175005, INDIA
sudebmajee@gmail.com

Rajendra K. Ray
School of Basic Sciences
Indian Institute of Technology Mandi
PIN 175005, INDIA
rajendra@iitmandi.ac.in

Ananta K. Majee
Department of Mathematics
Indian Institute of Technology Delhi
PIN 110016, INDIA
majee@maths.iitd.ac.in

March 9, 2022

ABSTRACT

In this article, we consider a non-linear hyperbolic-parabolic coupled system based on telegraph diffusion framework applied to image despeckling. A separate equation is used to calculate the edge variable, which improves the quality of the despeckled images. A well-posedness result of the proposed coupled system is settled via Schauder's fixed point theorem. Numerical experiments are reported to illustrate the effectiveness of the proposed model, with recently developed models, over a set of gray level test images contaminated by speckle noise.

Keywords Speckle noise · Despeckling · Telegraph diffusion equation · Coupled System · Well-posedness · Schauder fixed point theorem.

1 Introduction

Beginning with the Perona-Malik model [23], non-linear partial differential equations (PDEs) are extensively used to develop noise reduction models. Due to the availability of well established numerical schemes and theoretical properties, PDE based image processing is an exciting research area for real-life application purpose as well as for the theoretical study. In the real situation, images are often degraded by different types of noises, e.g., additive, multiplicative, or mixed nature. Hence the noise extraction is a very initial stage for high-level image analysis. In this work, we only consider the multiplicative speckle [22] noise removal process. A Mathematical representation for a degraded image affected by speckle noise[7] can be expressed as

$$J = I\eta,$$

where J is the noisy image, I is the noise-free image, and η signifies the speckle-noise process.

In general, the speckle noise process η is Gamma(L, L) distributed, where $L \in \mathbb{N}$ is the the number of looks corresponding to the noise level in the corrupted images [2, 10, 19]. To remove speckle based noise in the images, different types of PDE based models are proposed and resulted in significant momentum both in the development of theoretical as well as numerical aspects of the problems. Most popular PDE based approaches are anisotropic diffusion-based

methods [13, 14, 16, 26, 31, 33, 34], and variational methods [3, 6, 11, 15, 17, 18, 20, 25, 27]. Most of the above models take the generalized form

$$I_t = \text{div}(g(t, x) \nabla I) + \lambda f(J, I) \quad \text{in } \Omega_T := (0, T) \times \Omega, \quad (1.1)$$

with the appropriate initial and boundary conditions. Here Ω is the domain of the original image I and the observed noisy image J , T is a specified time, λ is the weight parameter, div and ∇ represents the divergence and gradient operator respectively. The source term $f(J, I)$ is derived from the variational model approach [3, 6, 18, 25]. In (1.1), $g(t, x)$ signifies the degree of denoising which preserves the image characteristics, e.g., textures and edges in the noise removal process. All the above-discussed PDE based models are parabolic type.

Later, V. Ratner, and Y. Zeevi [24] introduces the idea of hyperbolic PDE for additive noise removal process. By considering the image as an elastic sheet, the authors in [24] suggest the following telegraph diffusion equation (TDE) based model

$$I_{tt} + \gamma I_t - \text{div} \left(\frac{\nabla I}{1 + \frac{|\nabla I|^2}{K}} \right) = 0, \quad \text{in } \Omega_T,$$

where γ is the damping parameter and K is a threshold constant. Even though the TDE model can effectively preserve the sharp edges but failed to produce satisfactory smoothing in the presence of a large level of noise. To overcome this issue, several non-linear telegraph diffusion-based method have been proposed [4, 12, 28, 30, 32]. However, in spite of their impressive applications in the field of additive noise removal process, hyperbolic PDE based approaches have not successfully used for speckle noise removal process. Recently Sudeb et al. suggest a couple of hyperbolic PDE based models [21, 22] for speckle noise removal process. The authors in [21] developed a model in a telegraph total variation framework as

$$\begin{aligned} I_{tt} + \gamma I_t &= \text{div} \left(\theta(I) \frac{\nabla I}{|\nabla I|} \right) - \lambda \left(1 - \frac{J}{I} \right), & \text{in } \Omega_T, \\ \partial_n I &= 0, & \text{in } \partial\Omega_T := (0, T) \times \partial\Omega, \\ I(0, x) &= J(x), \quad I_t(0, x) = 0, & \text{in } \Omega, \end{aligned}$$

where θ is the fuzzy edge detector function [5]. In [22], the authors developed a model in a telegraph diffusion based framework of the form

$$I_{tt} + \gamma I_t - \text{div} (g(I_\xi, |\nabla I_\xi|) \nabla I) = 0, \quad \text{in } \Omega_T,$$

with the similar initial and boundary conditions as in [21], where the diffusion control function g is given by

$$g(I_\xi, |\nabla I_\xi|) = \frac{2|I_\xi|^\nu}{(M_\xi^I)^\nu + |I_\xi|^\nu} \cdot \frac{1}{1 + \left(\frac{|\nabla I_\xi|}{K} \right)^2}.$$

In the above, $I_\xi = G_\xi * I$, $M_\xi^I = \max_{x \in \Omega} |I_\xi(t, x)|$, $\nu \geq 1$, $\xi > 0$, and “ $*$ ” represents convolution in x only and G_ξ is a two dimensional Gaussian kernel.

To the best of our knowledge, most of the PDE based models for speckle noise removal are single and parabolic types. Inspired by the ideas of [14, 22], we propose the following improved nonlinear and coupled hyperbolic-parabolic model

$$I_{tt} + \gamma I_t - \text{div} \left(\frac{s^\alpha}{1 + s^\alpha} \frac{1}{1 + \iota |u_\xi|^\beta} \nabla I \right) = 0, \quad \text{in } \Omega_T, \quad (1.2)$$

$$u_t = h(|\nabla I_\xi|) - u + \frac{\nu^2}{2} \Delta u, \quad \text{in } \Omega_T, \quad (1.3)$$

$$\begin{cases} I(0, x) = I_0(x), \quad I_t(0, x) = 0, \quad u(0, x) = G_\xi * |\nabla I_0|^2 \\ \partial_n I = 0 = \partial_n u \end{cases} \quad \begin{matrix} \text{in } \Omega, \\ \text{on } \partial\Omega_T, \end{matrix} \quad (1.4)$$

with $s := \frac{|I_\xi|}{M_\xi^I} \in [0, 1]$. In the above, I_0 is the observed noisy image, $\alpha \geq 1$, $\beta \geq 1$, $\gamma > 0$, $\nu > 0$, and $\iota > 0$ are constants. Δ is Laplace operator, $h : \mathbb{R}^+ \rightarrow \mathbb{R}^+$ is a bounded, Lipschitz continuous function. Moreover, u represents the edge strength at each scale. Here we utilize an extra equation to calculate the edge variable, which improves the present model over our previous model [22]. For simulation purpose, we opt an explicit numerical method to solve the present model and then apply it on different types of gray level test images. A comparison study regarding the

quality of the despeckled image is carried out with recently developed models [22, 26]. Moreover, we compare the quantitative and qualitative results at different noise levels.

The rest of the paper is organized as follows. In section 2, we study the wellposedness of the proposed model. Section 3 describes the numerical implementation and despeckling performance of the proposed model. We conclude the paper in Section 4 with a scope on future work.

2 Existence and Uniqueness of weak solution

This section is devoted to the wellposedness result of the proposed system (1.2)-(1.4). Due to the nonlinearity in the system (1.2)-(1.4), we first consider the associated linearized problem and then use Schauder's fixed-point theorem [8] to complete the proof. Without loss of generality, we assume that $\gamma = 1$, $\iota = 1$, and $\nu = 1$ in the equations (1.2) and (1.3).

2.1 Technical framework and statement of the main result

Throughout this article, we consider $C > 0$ as a generic constant. By $(L^p, \|\cdot\|_{L^p})$ with $1 \leq p \leq \infty$, we denote the standard spaces of p -th order integrable functions on Ω . Moreover, for $r \in \mathbb{N}$ we write $(H^r, \|\cdot\|_{H^r})$ as the usual Sobolev spaces on Ω , and $(H^1)'$ as the dual space of H^1 . We consider the solution space $W(0, T)$ for the underlying problem (1.2)-(1.4) as $W(0, T) = W_1(0, T) \times W_2(0, T)$, where

$$\begin{aligned} W_1(0, T) &= \left\{ w \in L^\infty(0, T; H^1), w_t \in L^\infty(0, T; L^2); w_{tt} \in L^2(0, T; (H^1)') \right\}, \\ W_2(0, T) &= \left\{ w : w \in L^\infty(0, T; H^1); w_t \in L^\infty(0, T; L^2) \right\}. \end{aligned}$$

Definition 2.1 (Weak solution) A pair (I, u) is said to be a weak solution of (1.2)-(1.4), if

- a) $I \in W_1(0, T)$, $u \in W_2(0, T)$ and (1.4) holds.
- b) For all $\phi \in H^1$ and a.e $t \in (0, T)$, there hold

$$\begin{aligned} \langle I_{tt}, \phi \rangle + \int_{\Omega} I_t \phi \, dx + \int_{\Omega} \frac{s^\alpha}{1 + s^\alpha} \frac{1}{1 + |u_\xi|^\beta} \nabla I \cdot \nabla \phi \, dx &= 0, \\ \int_{\Omega} u_t \phi \, dx + \frac{1}{2} \int_{\Omega} \nabla u \cdot \nabla \phi \, dx + \int_{\Omega} u \phi \, dx &= \int_{\Omega} h(|\nabla I_\xi|) \phi \, dx. \end{aligned}$$

Theorem 2.1 The system (1.2)-(1.4) admits a unique weak solution $(I, u) \in W$ in the sense of Definition 2.1, provided the following two conditions hold:

A.1 $I_0 \in H^2$ satisfying $0 < \rho := \inf_{x \in \Omega} I_0(x)$.

A.2 $h : \mathbb{R}^+ \rightarrow \mathbb{R}^+$ is a bounded, Lipschitz continuous function with Lipschitz constant c_h such that

$$0 \leq h(\tilde{u}) \leq 1 \quad \forall \tilde{u} \in \mathbb{R}^+.$$

2.2 Linearized problem & its Well-posedness

For any positive constants $M_1, M_2 > 0$, define the convex set

$$\mathcal{B}_{M_1, M_2} = \left\{ \begin{array}{l} \bar{I} \in W_1(0, T) : \quad \|\bar{I}\|_{L^\infty(0, T; H^1)} + \|\bar{I}_t\|_{L^\infty(0, T; L^2)} \leq M_1 \|I_0\|_{H^1}, \\ 0 < \rho \leq \bar{I}(t, x) \text{ for a.e. } (t, x) \in \Omega_T, \\ \bar{u} \in W_2(0, T) : \quad \|\bar{u}\|_{L^\infty(0, T; L^2)} + \|\bar{u}_t\|_{L^\infty(0, T; L^2)} \leq M_2 \|I_0\|_{L^2}. \end{array} \right.$$

For any fixed $(\bar{I}, \bar{u}) \in \mathcal{B}_{M_1, M_2}$, consider the linearized problem:

$$I_{tt} + I_t - \operatorname{div}(\bar{g}(t, x) \nabla I) = 0 \quad \text{in } \Omega_T, \quad (2.1)$$

$$u_t = h(|\nabla \bar{I}_\xi|) - u + \frac{1}{2} \Delta u \quad \text{in } \Omega_T, \quad (2.2)$$

with the condition (1.4), where the function \bar{g} is given by

$$\bar{g}(t, x) \equiv g_{\bar{I}, \bar{u}}(t, x) := \frac{|\bar{I}_\xi|^\alpha}{(M_\xi^\alpha)^\alpha + |\bar{I}_\xi|^\alpha} \cdot \frac{1}{1 + |\bar{u}_\xi|^\beta}.$$

Since $(\bar{I}, \bar{u}) \in \mathcal{B}_{M_1, M_2}$, a similar argument as in the proof of [22, Claim 2.1] reveals that

$$\begin{aligned} \text{i) } & 0 < \kappa \leq \bar{g} \leq 1, \\ \text{ii) } & |\bar{g}_t| \leq C, \end{aligned} \tag{2.3}$$

where $\kappa, C > 0$ are constants depending only on $G_\xi, I_0, M_1, M_2, \beta, \alpha$ and ρ . Hence, thanks to the classical Galerkin method [8], one can show that there exists a unique weak solution $(I, u) \in W(0, T)$ of the linearized problem (2.1)-(2.2) with the condition (1.4).

Lemma 2.2 *The unique solution $(I, u) \in W(0, T)$ of the linearized problem (2.1)-(2.2) with the condition (1.4) satisfies the following:*

$$\text{a) } \|I\|_{L^\infty(0, T; H^1)} + \|I_t\|_{L^\infty(0, T; L^2)} \leq C\|I_0\|_{H^1},$$

$$\text{b) } \int_0^T \|I_{tt}\|_{(H^1)}^2 dt \leq CT\|I_0\|_{H^1}^2,$$

$$\text{c) } \|u\|_{L^\infty(0, T; H^1)} + \|u_t\|_{L^\infty(0, T; L^2)} \leq C\|I_0\|_{H^1},$$

where $C > 0$ is a constant, depends only on $G_\xi, I_0, h, M_1, M_2, \alpha, \beta$ and ρ .

Proof: Since $\|\bar{u}_t\|_{L^\infty(0, T; L^2)} \leq C\|I_0\|_{H^1}$, by following computations as in Sudeb et al. [22, Lemma 3.2], one can show the validation of the estimates a) and b) of Lemma 2.2. To prove c), we proceed as follows: multiply (2.2) by u_t , integrate by parts over Ω , use Cauchy-Schwarz and Young's inequalities, and then integrate w.r.t time between 0 to t . We have, for a.e. $t \in (0, T)$

$$\|u\|_{H^1}^2 + \int_0^t \|u_t\|_{L^2}^2 ds \leq C(1 + t|\Omega|).$$

Moreover, since $u_0 \in H^2$ and $\bar{h}_t \in L^\infty(0, T; L^2)$, by regularity theory [8], $u_t \in L^\infty(0, T; L^2)$ with

$$\|u\|_{H^1}^2 + \|u_t\|_{L^2}^2 \leq C e^t (1 + t|\Omega|). \tag{2.4}$$

Hence c) of Lemma 2.2 follows from (2.4).

2.3 Proof of Theorem 2.1

As mentioned earlier, we show the well-posedness of the system (1.2)-(1.4) via Schauder's fixed-point theorem. To do so, we introduce a non-empty, convex and weakly compact subset W_0 of $W(0, T)$ defined by

$$W_0 = \left\{ (w, v) \in W(0, T) : \begin{aligned} & \|w\|_{L^\infty(0, T; H^1)} + \|w_t\|_{L^\infty(0, T; L^2)} \leq C\|I_0\|_{H^1}^2, \\ & \|v\|_{L^\infty(0, T; H^1)} + \|v_t\|_{L^\infty(0, T; L^2)} \leq C\|I_0\|_{H^1}; \\ & 0 < \rho \leq w(t, x) \text{ for a.e. } (t, x) \in \Omega_T, \text{ and } (w, v) \text{ satisfies (1.4)} \end{aligned} \right\}.$$

Consider a mapping

$$\begin{aligned} \mathcal{P} : W_0 &\rightarrow W_0 \\ (w, v) &\mapsto (I_w, u_v). \end{aligned}$$

If we show that the mapping $\mathcal{P} : (w, v) \rightarrow (I_w, u_v)$ is weakly continuous from W_0 into W_0 , then by Schauder's fixed-point theorem, there exists $(w, v) \in W_0$ such that $(w, v) = \mathcal{P}(w, v)$. In other words, the coupled system (1.2)-(1.3) has a weak solution. In order to prove weak continuity of \mathcal{P} , let (w_k, v_k) be a sequence that converges weakly to

some (w, v) in W_0 and let $(I_k, u_k) = (I_{w_k}, u_{v_k})$. We have to show that $\mathcal{P}(w_k, v_k) := (I_k, u_k)$ converges weakly to $\mathcal{P}(w, v) := (I_w, u_v)$.

Thanks to Lemma 2.2, one can use classical results of compact inclusion in Sobolev spaces [1] to extract subsequences $\{w_{k_n}\}$ of $\{w_k\}$, $\{v_{k_n}\}$ of $\{v_k\}$, $\{I_{k_n}\}$ of $\{I_k\}$ and $\{u_{k_n}\}$ of $\{u_k\}$, still denoted by same sequences $\{w_k\}$, $\{v_k\}$, $\{I_k\}$ and $\{u_k\}$, such that for some $(I, u) \in W_0$, the followings hold as $k \rightarrow \infty$:

$$\begin{aligned}
w_k &\rightarrow w, \quad v_k \rightarrow v \quad \text{in } L^2(0, T; L^2) \quad \text{and a.e. on } \Omega_T, \\
G_\xi * w_k &\rightarrow G_\xi * w \quad \text{in } L^2(0, T; L^2) \quad \text{and a.e. on } \Omega_T, \\
|G_\xi * w_k|^\alpha &\rightarrow |G_\xi * w|^\alpha \quad \text{in } L^2(0, T; L^2) \quad \text{and a.e. on } \Omega_T, \\
\frac{|G_\xi * w_k|^\alpha}{(M_\xi^{w_k})^\alpha + |G_\xi * w_k|^\alpha} &\rightarrow \frac{|G_\xi * w|^\alpha}{(M_\xi^w)^\alpha + |G_\xi * w|^\alpha} \quad \text{in } L^2(0, T; L^2) \quad \text{and a.e. on } \Omega_T, \\
\partial_{x_i} G_\xi * w_k &\rightarrow \partial_{x_i} G_\xi * w \quad (i = 1, 2) \quad \text{in } L^2(0, T; L^2) \quad \text{and a.e. on } \Omega_T, \\
h(|\nabla G_\xi * w_k|) &\rightarrow h(|\nabla G_\xi * w|) \quad \text{in } L^2(0, T; L^2) \quad \text{and a.e. on } \Omega_T, \\
|G_\xi * v_k| &\rightarrow |G_\xi * v| \quad \text{in } L^2(0, T; L^2) \quad \text{and a.e. on } \Omega_T, \\
\frac{1}{1 + |G_\xi * v_k|^\beta} &\rightarrow \frac{1}{1 + |G_\xi * v|^\beta} \quad \text{in } L^2(0, T; L^2) \quad \text{and a.e. on } \Omega_T, \\
I_k &\rightarrow I, \quad u_k \rightarrow u \quad \text{weakly* in } L^\infty(0, T; H^1), \\
I_k &\rightarrow I, \quad u_k \rightarrow u \quad \text{in } L^2(0, T; L^2), \\
\partial_t I_k &\rightarrow \partial_t I, \quad \partial_t u_k \rightarrow \partial_t u \quad \text{weakly* in } L^\infty(0, T; L^2), \\
\partial_{tt} I_k &\rightarrow \partial_{tt} I \quad \text{weakly* in } L^2(0, T; (H^1)').
\end{aligned}$$

In view of the above convergences, one can pass to the limit in (2.1)-(2.2) and obtain $(I, u) = \mathcal{P}(w, v)$. Moreover, since the solution of (2.1)-(2.2) is unique, the whole sequence $(I_k, u_k) = \mathcal{P}(w_k, v_k)$ converges weakly in W_0 to $(I, u) = \mathcal{P}(w, v)$. Hence \mathcal{P} is weakly continuous. Therefore, the problem (1.2)-(1.4) admits a weak solution.

Uniqueness of weak solution: To prove the uniqueness of weak solutions of the underlying problem (1.2)-(1.4), we use here a standard methodology [8]. Let (I_1, u_1) and (I_2, u_2) be two weak solutions of (1.2)-(1.4). Then, we have

$$I_{tt} + I_t - \operatorname{div}(g_{I_1, u_1} \nabla I) = \operatorname{div}((g_{I_1, u_1} - g_{I_2, u_2}) \nabla I_2) \quad \text{in } \Omega_T, \quad (2.5)$$

$$u_t - \Delta u + u = h(|\nabla G_\xi * I_1|) - h(|\nabla G_\xi * I_2|) \quad \text{in } \Omega_T, \quad (2.6)$$

$$\begin{cases} I(0, x) = 0, \quad I_t(0, x) = 0, \quad u(0, x) = 0 \\ \partial_n I = 0 = \partial_n u \end{cases} \quad \begin{matrix} \text{in } \Omega, \\ \text{on } \partial\Omega_T, \end{matrix} \quad (2.7)$$

where $I = I_1 - I_2$ and $u = u_1 - u_2$. It suffices to show that $(I, u) \equiv (0, 0)$. To verify this, fix $0 < s < T$, and set for $i = 1, 2$,

$$v_i(t, \cdot) = \begin{cases} \int_t^s I_i(\tau, \cdot) d\tau, & 0 < t \leq s, \\ 0 & s \leq t < T. \end{cases} \quad (2.8)$$

Note that, for $t \in (0, T)$,

$$\begin{cases} \partial_t v_i(t, x) = -I_i(t, x) & i = 1, 2, \\ v_i(t, \cdot) \in H^1, \quad \partial_n v_i = 0 & \text{on } \partial\Omega \text{ in the sence of distribution.} \end{cases} \quad (2.9)$$

Set $v = v_1 - v_2$. Then $v(s, \cdot) = 0$. Now one can follow the same argumentation as in [22, Section 3.3] to arrive at

$$\begin{aligned}
&\frac{1}{2} \|I(s)\|_{L^2}^2 + \int_0^s \|I(t)\|_{L^2}^2 dt + \frac{1}{2} \int_\Omega g_{I_1, u_1}(0, x) |\nabla v(0, x)|^2 dx \\
&\leq \frac{1}{2} \left| \int_0^s \int_\Omega |\nabla v|^2 \partial_t g_{I_1, u_1} dx dt \right| + \int_0^s \|(g_{I_1, u_1} - g_{I_2, u_2})(t)\|_{L^\infty} \|\nabla I_2(t)\|_{L^2} \|\nabla v(t)\|_{L^2} dt.
\end{aligned} \quad (2.10)$$

Like in (2.3), there exist positive constants $\kappa_1, C_1 > 0$ such that

$$\kappa_1 \leq g_{I_1, u_1} \leq 1, \quad |\partial_t g_{I_1, u_1}| \leq C.$$

Moreover, by using property of convolution and the positive lower bound ρ of the solutions I_i , we get

$$\|(g_{I_1, u_1} - g_{I_2, u_2})(t)\|_{L^\infty} \leq C(\xi, \alpha, I_0, \rho)(\|I(t)\|_{L^2}^\alpha + \|u\|_{L^2}).$$

Thus we have, from (2.10)

$$\begin{aligned} \frac{1}{2}\|I(s)\|_{L^2}^2 + \int_0^s \|I(t)\|_{L^2}^2 dt + C\|\nabla v(0)\|_{L^2}^2 &\leq C\left(\int_0^s (\|\nabla v(t)\|_{L^2}^2 + \|I(t)\|_{L^2}^{2\alpha} + \|u(t)\|_{L^2}^2) dt\right) \\ &\leq C\left(\int_0^s (\|v(t)\|_{H^1}^2 + \|I(t)\|_{L^2}^2 + \|u(t)\|_{L^2}^2) dt\right), \end{aligned}$$

where in the last inequality, we have used the fact that $\alpha \geq 1$. Set

$$w_i(t, \cdot) = \int_0^t I_i(\tau, \cdot) d\tau; \quad w(t, \cdot) = (w_1 - w_2)(t, \cdot), \quad 0 < t \leq T.$$

Then, by using a similar argument as in [22, Section 3.3], we obtain

$$\begin{aligned} \frac{1}{2}\|I(s)\|_{L^2}^2 + \int_0^s \|I(t)\|_{L^2}^2 dt + C\|w(s)\|_{H^1}^2 \\ \leq \tilde{C}s\|w(s)\|_{H^1}^2 + C\int_0^s (\|w(t)\|_{H^1}^2 + \|I(t)\|_{L^2}^2 + \|u(t)\|_{L^2}^2) dt. \end{aligned}$$

Choose T_1 sufficiently small such that $C - \tilde{C}T_1 > 0$. Then, for $0 < s \leq T_1$, we have

$$\|I(s)\|_{L^2}^2 + \|w(s)\|_{H^1}^2 \leq C\int_0^s (\|w(t)\|_{H^1}^2 + \|I(t)\|_{L^2}^2 + \|u(t)\|_{L^2}^2) dt. \quad (2.11)$$

Now, by multiplying (2.6) by u and integrating over Ω , we have

$$\frac{d}{dt}\|u\|_{L^2}^2 + 2\|\nabla u\|_{L^2}^2 \leq C\left(\|h(|\nabla G_\xi * I_1|) - h(|\nabla G_\xi * I_2|)\|_{L^2}^2 + \|u\|_{L^2}^2\right).$$

Since h is Lipschitz continuous, by using Young's inequality for convolution, we see that

$$\|h(|\nabla G_\xi * I_1|) - h(|\nabla G_\xi * I_2|)\|_{L^2}^2 \leq C(c_h, \xi)\|I\|_{L^2}^2.$$

Thus, we have, for $0 < s \leq T_1$,

$$u(s) \leq C\int_0^s \|I(t)\|_{L^2}^2 dt. \quad (2.12)$$

Adding (2.11) and (2.12), we finally get, for $0 < s \leq T_1$,

$$\|I(s)\|_{L^2}^2 + \|u(s)\|_{L^2}^2 + \|w(s)\|_{H^1}^2 \leq C\int_0^s (\|w(t)\|_{H^1}^2 + \|I(t)\|_{L^2}^2 + \|u(t)\|_{L^2}^2) dt.$$

Hence by Gronwall's lemma, we see that $(I, u) \equiv (0, 0)$ on $[0, T_1]$. We repeatedly use the above argument on the intervals $(T_1, 2T_1]$, $(2T_1, 3T_1]$, \dots step by step, and arrive at the conclusion that $I_1 = I_2$ and $u_1 = u_2$ on $(0, T)$. This completes the proof of Theorem 2.1.

For any weak solution (I, u) of (1.2)-(1.4), we next show the boundedness of I under the assumption that initial image I_0 has a finite upper bound, whose proof follows from the proof of [22, Lemma 3.3].

Lemma 2.3 *Let (I, u) be a weak solution of the system (1.2)-(1.4), and $\varrho := \sup_{x \in \Omega} I_0(x) < \infty$. Then*

$$0 < \rho \leq I(t, x) \leq \varrho \quad \text{for a.e. } (t, x) \in \Omega_T. \quad (2.13)$$

3 Numerical method and Experimental Results

In this section, we show the image despeckling performance of the suggested model over two existing approaches [22, 26]. To solve the model (1.2)-(1.4) numerically, we opt an explicit finite difference scheme. We replace the derivative terms in the model (1.2)-(1.4) using the following finite difference formulas:

$$\frac{\partial I_{i,j}^n}{\partial t} \approx \frac{I_{i,j}^{n+1} - I_{i,j}^n}{\tau}, \quad \frac{\partial^2 I_{i,j}^n}{\partial t^2} \approx \frac{I_{i,j}^{n+1} - 2I_{i,j}^n + I_{i,j}^{n-1}}{\tau^2},$$

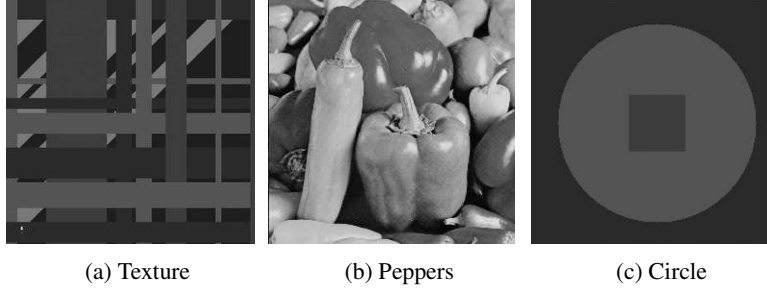


Figure 1: Test Images: (a) Texture Image, (b) Natural Image, (c) Synthetic Image.

$$\begin{aligned}\nabla_x I_{i,j}^n &\approx \frac{I_{i+1,j}^n - I_{i-1,j}^n}{2\tilde{h}}, \quad \nabla_y I_{i,j}^n \approx \frac{I_{i,j+1}^n - I_{i,j-1}^n}{2\tilde{h}}, \\ \Delta_x I_{i,j}^n &\approx \frac{I_{i+1,j}^n - 2I_{i,j}^n + I_{i-1,j}^n}{\tilde{h}^2}, \quad \Delta_y I_{i,j}^n \approx \frac{I_{i,j+1}^n - 2I_{i,j}^n + I_{i,j-1}^n}{\tilde{h}^2}, \\ |\nabla I_{i,j}^n| &\approx \sqrt{(\nabla_x I_{i,j}^n)^2 + (\nabla_y I_{i,j}^n)^2}.\end{aligned}$$

In the above, τ resp. \tilde{h} denotes the time step size resp. the spatial step size. $I_{i,j}^n = I(t_n, x_i, y_j)$ where $x_i = i\tilde{h}$ ($i = 0, 1, 2, \dots, N$), $y_j = j\tilde{h}$ ($j = 0, 1, 2, \dots, M$), $t_n = n\tau$ ($n = 0, 1, 2, \dots$) where n is the number of iterations and $M \times N$ is the image dimension. Then, the discrete form of the equation (1.2) could be written as

$$(1 + \gamma\tau)I_{i,j}^{n+1} = (2 + \gamma\tau)I_{i,j}^n - I_{i,j}^{n-1} + \tau^2 \{ \nabla_x (g_{i,j}^n \nabla_x I_{i,j}^n) + \nabla_y (g_{i,j}^n \nabla_y I_{i,j}^n) \}, \quad (3.1)$$

where

$$g_{i,j}^n = b(s_{i,j}^n) \cdot \frac{1}{1 + \iota |G_\xi * u_{i,j}^n|^\beta} \quad \text{with } b(s) = \frac{s^\alpha}{1 + s^\alpha}.$$

Moreover, $u(t_n, x_i, y_j) = u_{i,j}^n$ is calculated from the discretized equation of (1.3) as follows

$$u_{i,j}^n = u_{i,j}^{n-1} + \tau \{ h_{i,j}^n - u_{i,j}^{n-1} + \frac{\nu^2}{2} (\Delta_x u_{i,j}^{n-1} + \Delta_y u_{i,j}^{n-1}) \}, \quad (3.2)$$

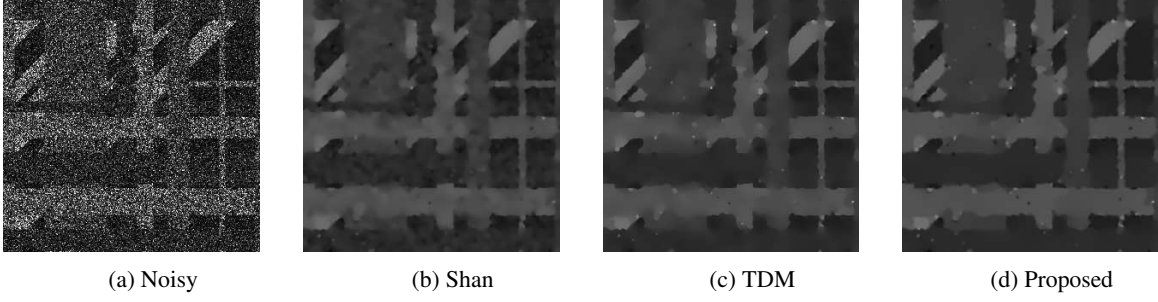
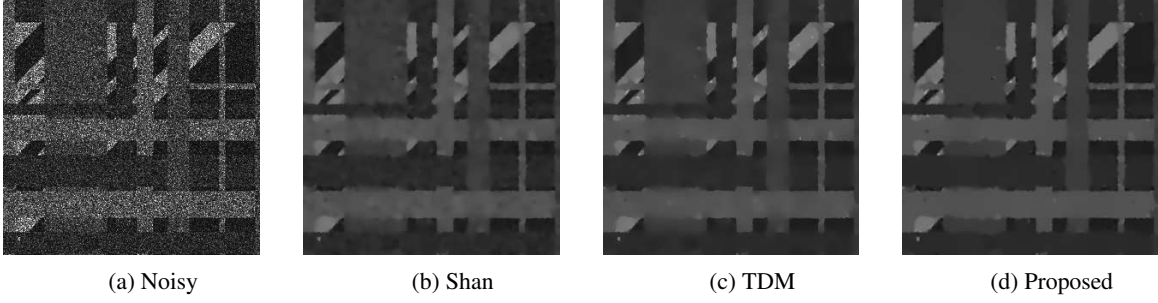
where $h_{i,j}^n = h(|\nabla(G_\xi * I_{i,j}^n)|)$. We choose the function h as $h(\theta) = \epsilon + \min\{\theta^2, K\}$ for numerical experiments, where K is square of the maximum gray level value of the image I and $\epsilon > 0$ is a very small number. The boundary and initial conditions are given as follows:

$$\begin{aligned}I_{-1,j}^n &= I_{0,j}^n, \quad I_{N+1,j}^n = I_{N,j}^n, \quad I_{i,-1}^n = I_{i,0}^n, \quad I_{i,M+1}^n = I_{i,M}^n, \\ I_{i,j}^0 &= I_0(x_i, y_j), \quad I_{i,j}^1 = I_{i,j}^0, \quad 0 \leq i \leq N, \quad 0 \leq j \leq M.\end{aligned}$$

We choose similar boundary conditions for edge variable u , and $u_{i,j}^0 = G_\xi * |\nabla I_{i,j}^0|^2$. We start the simulation with the initial value I_0 and utilize the equations (3.1) and (3.2) repeatedly to find a sequence of values of $I(t, x)$; $t > 0$, which represents the filtered versions of I_0 . We made a stopping criterion for the noise elimination process when the best PSNR [9] value for the restored image $I(t, x)$ is reached.

We perform all the experiments on three standard test images 1, which are initially degraded with different level of speckle noise. All the numerical experiments are performed under windows 7 and MATLAB version *R2018b* running on a desktop with an Intel Core *i5* dual-core CPU at 2.53 GHz with 4 GB of memory. In this process, we use same numerical scheme as done it for the proposed model to discretize the considered existing models. We choose an uniform time step size $\tau = 0.2$, spatial step size $\tilde{h} = 1$, and $\xi = 1$ for each models.

To compare the quantitative results, we compute the values of the two standard parameters PSNR[9] and MSSIM [29]. A higher numerical value of MSSIM and PSNR suggests that the despeckled image is closer to the noise-free image. Apart from the despeckled image, for qualitative observations, we compute the 2D contour plot, 3D surface plot for the better visualization of the computational results. In figures 2-4, we represent the restored results of a Texture image which is contaminated by multiplicative speckle noise with $L = \{1, 3, 5\}$. From figure 2b, we can see that the Shan model failed to preserve the fine edges for very high noise level. TDM model works better than the Shan model, but the present model preserves the fine edges better than Shan and TDM models.

Figure 2: Image corrupted with speckle look $L=1$ and restored by different models.Figure 3: Image corrupted with speckle look $L=3$ and restored by different models.

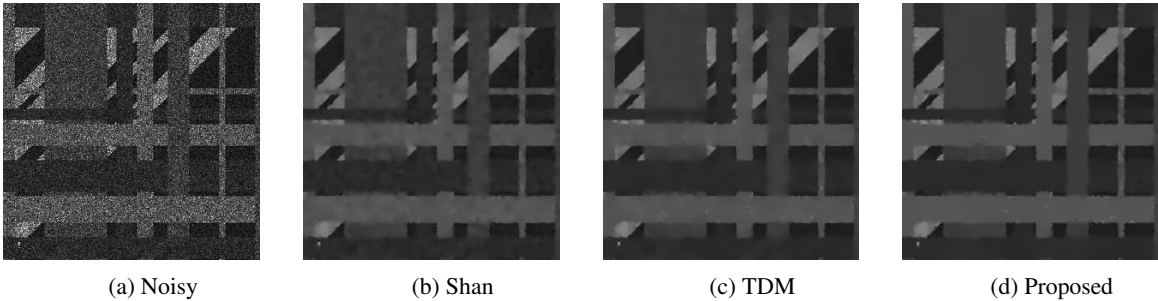
In figures 5-7, we represent the reconstructed results of a Peppers image (Natural Image) which is corrupted by speckle noise with $L = \{1, 3, 5\}$. From figure 5, we see that the present model leave less speckle than the other two models.

To check the more reconstruction ability of the present model in figures 8- 12 illustrate the qualitative results of a Circle image (Synthetic Image) which is corrupted by speckle noise with $L = \{1, 3, 5\}$.

In the figures 8- 10 we demonstrate the despeckled images, and in the figures 11-12 we illustrate the contour maps and 3D surface plots when the image is corrupted by $L = 5$. One can observe that from the contour maps, and 3D surface plots, Shan and TDM models left some speckles in the homogeneous regions, but the present model produces fewer artifacts with better edge preservation.

Computational Values of PSNR and MSSIM are presented in the Table 1. The highest values of PSNR and MSSIM for each noise level clearly shows that the suggested model is better than the other two models.

Conclusively, summarize the quantitative and qualitative results, we can confirm that the present model performance better than the other discussed models.

Figure 4: Image corrupted with speckle look $L=5$ and restored by different models.

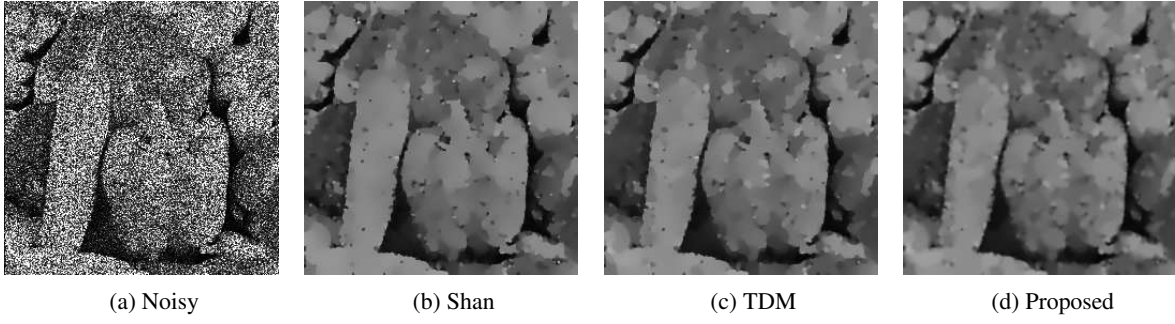


Figure 5: Image corrupted with speckle look $L=1$ and restored by different models.

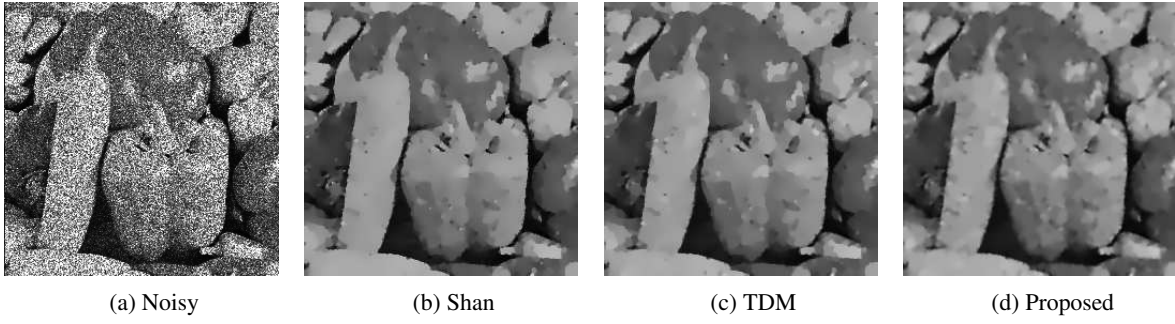


Figure 6: Image corrupted with speckle look $L=3$ and restored by different models.

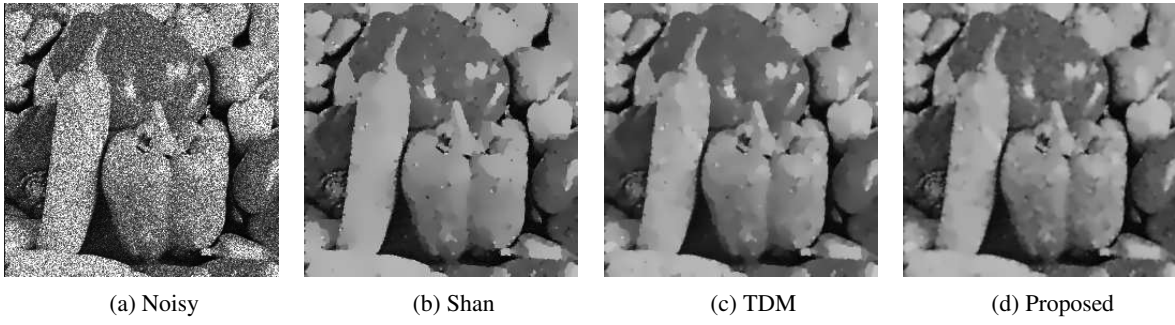


Figure 7: Image corrupted with speckle look $L=5$ and restored by different models.

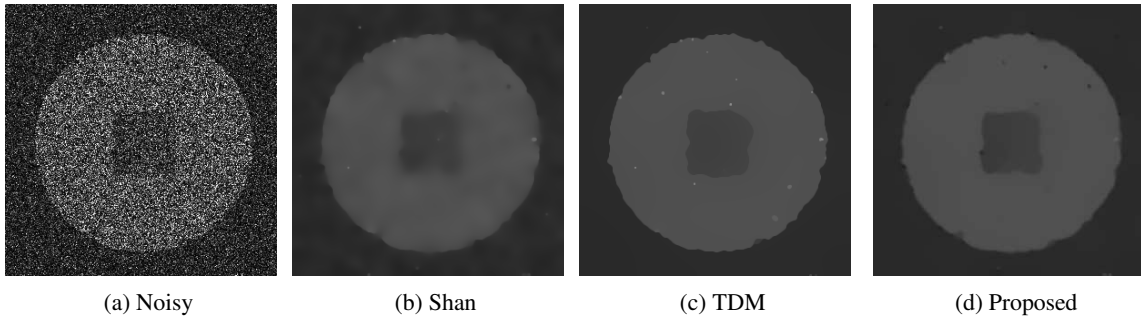


Figure 8: Image corrupted with speckle look $L=1$ and restored by different models.

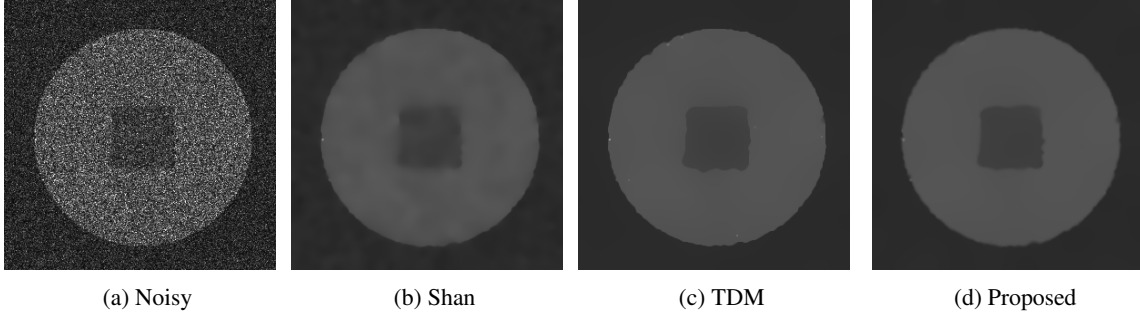


Figure 9: Image corrupted with speckle look $L=3$ and restored by different models.

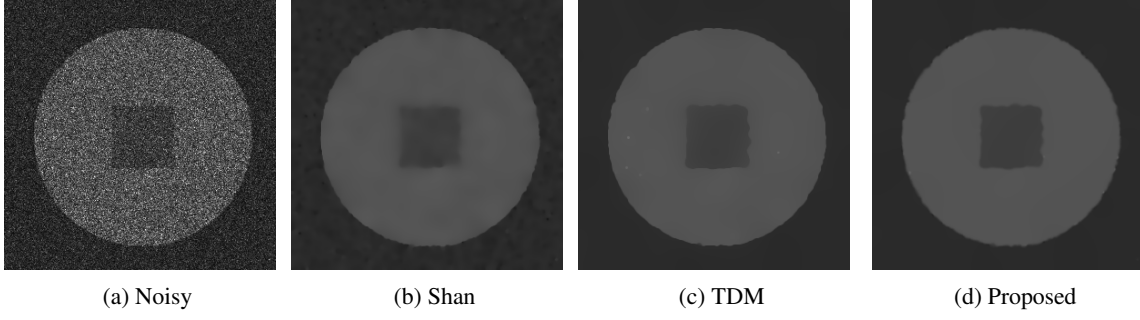


Figure 10: Image corrupted with speckle look $L=5$ and restored by different models.

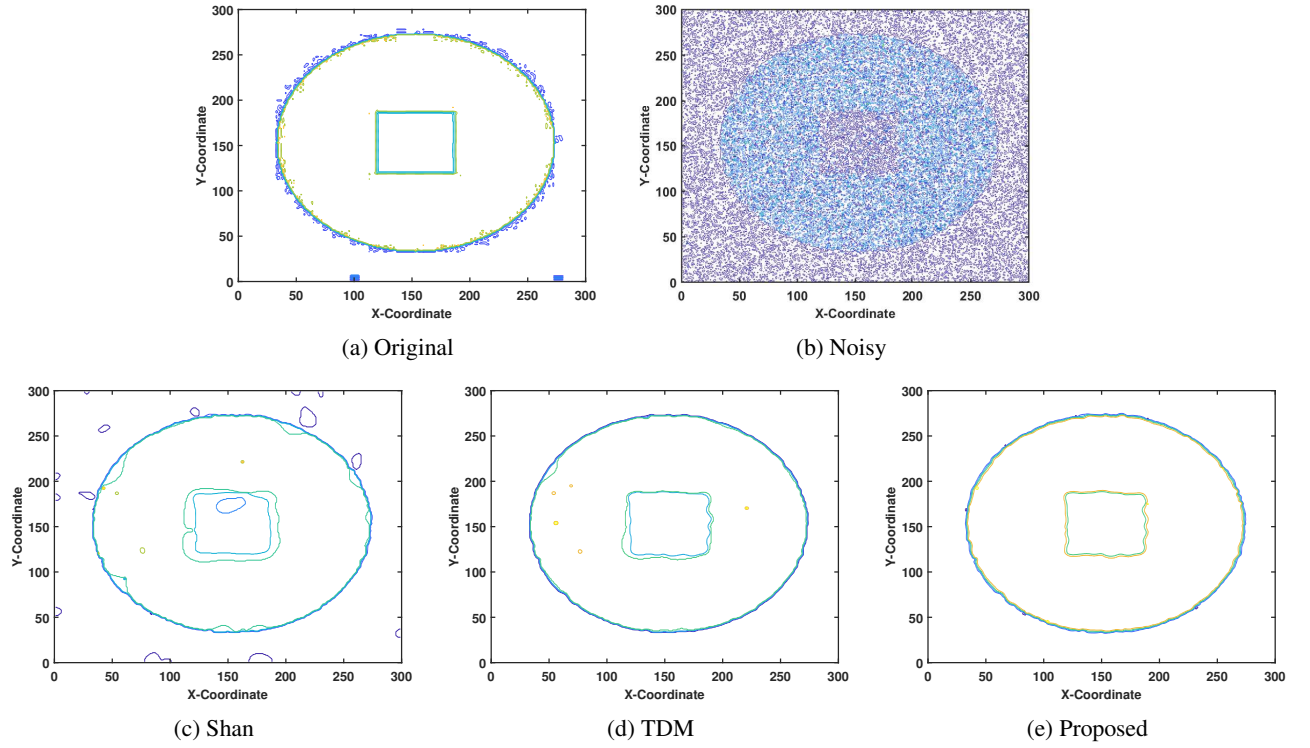


Figure 11: Contour plots of the restored images in figure 10.

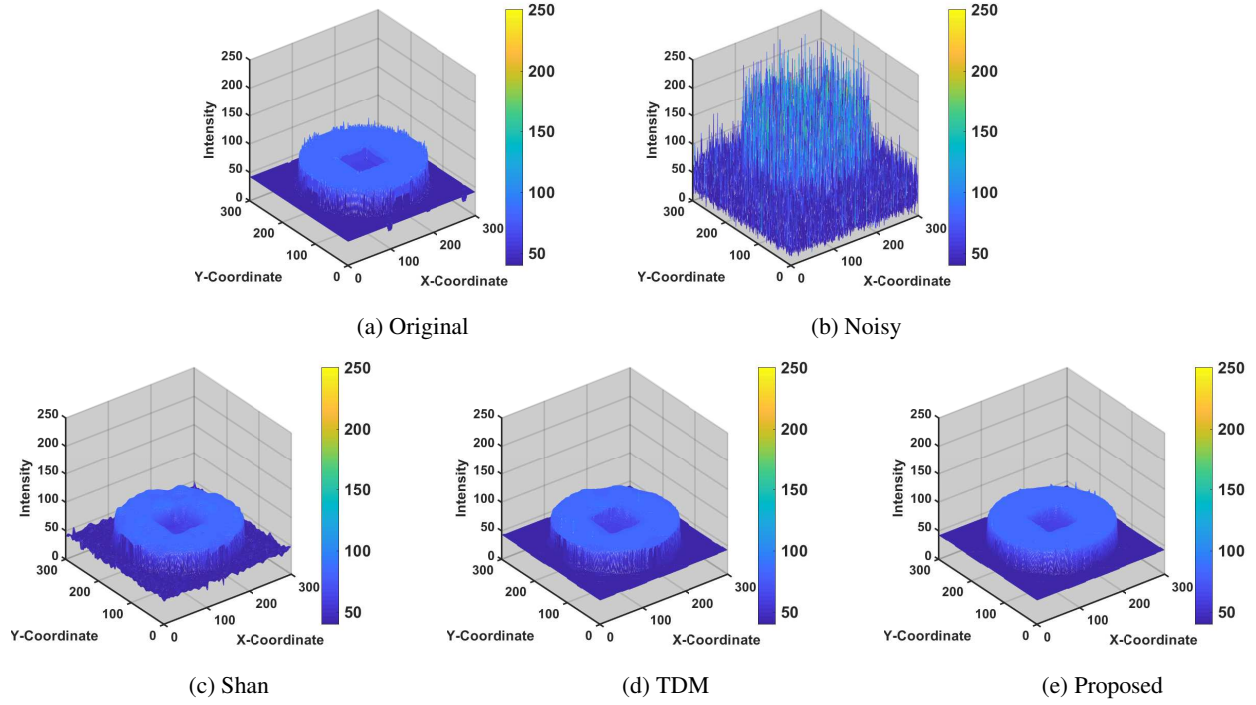


Figure 12: 3D surface plots of the restored images in figure 10.

Table 1: Left table: Comparison of MSSIM and PSNR values of despeckled images. Right table: Parameter values for the numerical experiments.

Image	L	Shan Model[26]		TDM [22]		Proposed Model	
		MSSIM	PSNR	MSSIM	PSNR	MSSIM	PSNR
Circle	1	0.9581	34.29	0.9643	34.69	0.9651	35.43
	3	0.9734	38.09	0.9771	39.52	0.9782	40.00
	5	0.9764	39.35	0.9805	40.72	0.9810	41.23
Texture	1	0.8125	27.61	0.8355	27.71	0.8360	27.83
	3	0.8782	30.83	0.8925	31.05	0.8967	31.31
	5	0.8979	31.87	0.9109	32.15	0.9164	32.47
Peppers	1	0.5827	17.56	0.5895	17.64	0.5905	17.83
	3	0.7018	22.46	0.7019	22.55	0.7061	22.85
	5	0.7155	23.73	0.7334	24.22	0.7395	24.67

Image	L	Shan[26]		TDM [22]			Proposed				
		α	β	γ	ν	K	γ	α	β	ϵ	ν
Circle	1	1.5	2	10	1	1	1	1.5	1.8	2.5	0.1
	3	1.5	2	10	1	1	2	1.7	2	2.5	0.1
	5	2	2.25	5	1	1	2	1.7	2.2	2	0.1
Texture	1	1.5	1.8	2	1.5	2	1	2	1	3	0.1
	3	1.8	2	2	1.5	2	2	2	1	3	0.1
	5	1.8	2	2	1.5	2	5	2.5	1	3	0.1
Peppers	1	1.5	2	1	1.5	2	1	2	1	3	0.1
	3	1.5	2	1	1.5	2	2	2	1	3	0.1
	5	2	2.4	2	1.5	2	2	2.5	1	3	0.1

4 Conclusion

In this work, we present a non-linear hyperbolic-parabolic coupled system applied to image despeckling. Such a improve method preserves the image characteristics in the noise removal process. To the best of our knowledge, coupled hyperbolic-parabolic PDE based model has not been used before for image speckle reduction. Moreover, we establish the well-posedness of the present model, show the boundedness of the weak solution. We compare the experimental results with two recently developed models and arrive at the conclusion that the proposed model well recovered the corrupted images without introducing undesired artifacts than that of existing models.

References

- [1] R. Adam, Sobolev spaces, in: Pure and Applied Mathematics Series of Monographs and Textbooks, Vol. 65, Academic Press, Inc., New York, San Francisco, London,, 1975.
- [2] Argenti, F., Lapini, A., Bianchi, T., Alparone, L.: A tutorial on speckle reduction in synthetic aperture radar images. IEEE Geoscience and remote sensing magazine 1(3), 6-35 (2013)

- [3] Aubert, G., Aujol, J.F.: A variational approach to removing multiplicative noise. *SIAM Journal on Applied Mathematics* 68(4), 925-946 (2008)
- [4] Cao, Y., Yin, J., Liu, Q., Li, M.: A class of nonlinear parabolic-hyperbolic equations applied to image restoration. *Nonlinear Analysis: Real World Applications* 11(1), 253-261 (2010)
- [5] Chaira, T., Ray, A.: A new measure using intuitionistic fuzzy set theory and its application to edge detection. *Applied soft computing* 8(2), 919-927 (2008)
- [6] Dong, G., Guo, Z., Wu, B.: A convex adaptive total variation model based on the gray level indicator for multiplicative noise removal. In: *Abstract and Applied Analysis*, vol. 2013. Hindawi Publishing Corporation (2013)
- [7] Dutt, V.: Statistical analysis of ultrasound echo envelope. *Ultrasound Research Laboratory* p. 181 (1995)
- [8] Evans, L.: *Partial Differential Equations*, in: *Graduate Studies in Mathematics*, vol. 19. American Mathematical Society, Providence, Rhode Island (1998)
- [9] Gonzalez, R.C., Woods, R.E.: *Digital image processing* (2002)
- [10] Hao, Y., Xu, J., Li, S., Zhang, X.: A variational model based on split bregman method for multiplicative noise removal. *AEU-International Journal of Electronics and Communications* 69(9), 1291-1296 (2015)
- [11] Huang, L.L., Xiao, L., Wei, Z.H.: Multiplicative noise removal via a novel variational model. *EURASIP Journal on image and video processing* 2010(1), 1 (2010)
- [12] Jain, S.K., Ray, R.K.: Edge detectors based telegraph total variational model for image filtering. In: *Information Systems Design and Intelligent Applications*, pp. 119-126. Springer (2016)
- [13] Jain, S.K., Ray, R.K.: Non-linear diffusion models for despeckling of images: achievements and future challenges. *IETE Technical Review* pp. 1-17 (2019)
- [14] Jain, S.K., Ray, R.K., Bhavsar, A.: A nonlinear coupled diffusion system for image despeckling and application to ultrasound images. *Circuits, Systems, and Signal Processing* pp. 1-30 (2018)
- [15] Jidesh, P., Bini, A.: A complex diffusion driven approach for removing data-dependent multiplicative noise. In: *International Conference on Pattern Recognition and Machine Intelligence*, pp. 284-289. Springer (2013)
- [16] Jin, J.S., Wang, Y., Hiller, J.: An adaptive nonlinear diffusion algorithm for filtering medical images. *IEEE Transactions on Information Technology in Biomedicine* 4(4), 298-305 (2000)
- [17] Jin, Z., Yang, X.: Analysis of a new variational model for multiplicative noise removal. *Journal of Mathematical Analysis and Applications* 362(2), 415-426 (2010)
- [18] Jin, Z., Yang, X.: A variational model to remove the multiplicative noise in ultrasound images. *Journal of Mathematical Imaging and Vision* 39(1), 62-74 (2011)
- [19] Liu, M., Fan, Q.: A modified convex variational model for multiplicative noise removal. *Journal of Visual Communication and Image Representation* 36, 187-198 (2016)
- [20] Liu, Q., Li, X., Gao, T.: A nondivergence p-laplace equation in a removing multiplicative noise model. *Nonlinear Analysis: Real World Applications* 14(5), 2046-2058 (2013)
- [21] Majee, S., Jain, S.K., Ray, R.K., Majee, A.K.: A fuzzy edge detector driven telegraph total variation model for image despeckling, a preprint arXiv <https://128.84.21.199/abs/1908.01134>, (2019)
- [22] Majee, S., Ray, R.K., Majee, A.K.: A gray level indicator-based regularized telegraph diffusion equation applied to image despeckling, a preprint arXiv <https://128.84.21.199/abs/1908.01147>, (2019).
- [23] Perona, P., Malik, J.: Scale-space and edge detection using anisotropic diffusion. *Pattern Analysis and Machine Intelligence, IEEE Transactions on* 12(7), 629-639 (1990)
- [24] Ratner, V., Zeevi, Y.Y.: Image enhancement using elastic manifolds. In: *Image Analysis and Processing, 2007. ICIAP 2007. 14th International Conference on*, pp. 769-774. IEEE (2007)
- [25] Rudin, L., Lions, P.L., Osher, S.: Multiplicative denoising and deblurring: Theory and algorithms. In: *Geometric Level Set Methods in Imaging, Vision, and Graphics*, pp. 103-119. Springer (2003)
- [26] Shan, X., Sun, J., Guo, Z.: Multiplicative noise removal based on the smooth diffusion equation. *Journal of Mathematical Imaging and Vision* pp. 1-17 (2019)
- [27] Shi, J., Osher, S.: A nonlinear inverse scale space method for a convex multiplicative noise model. *SIAM Journal on Imaging Sciences* 1(3), 294-321 (2008)
- [28] Sun, J., Yang, J., Sun, L.: A class of hyperbolic-parabolic coupled systems applied to image restoration. *Boundary Value Problems* 2016(1), 187 (2016)

- [29] Wang, Z., Bovik, A.C., Sheikh, H.R., Simoncelli, E.P.: Image quality assessment: from error visibility to structural similarity. *Image Processing, IEEE Transactions on* 13(4), 600-612 (2004)
- [30] Yang, Y.Q., Zhang, C.Y.: Kernel based telegraph-diffusion equation for image noise removal. *Mathematical Problems in Engineering* 2014 (2014)
- [31] Yu, Y., Acton, S.T.: Speckle reducing anisotropic diffusion. *IEEE Transactions on image processing* 11(11), 1260-1270 (2002)
- [32] Zhang, W., Li, J., Yang, Y.: Spatial fractional telegraph equation for image structure preserving denoising. *Signal Processing* 107, 368-377 (2015)
- [33] Zhou, Z., Guo, Z., Dong, G., Sun, J., Zhang, D., Wu, B.: A doubly degenerate diffusion model based on the gray level indicator for multiplicative noise removal. *IEEE Transactions on Image Processing* 24(1), 249-260 (2015)
- [34] Zhou, Z., Guo, Z., Zhang, D., Wu, B.: A nonlinear diffusion equation-based model for ultrasound speckle noise removal. *Journal of Nonlinear Science* 28(2), 443-470 (2018)